Available online at www.sciencedirect.com
SCIENCE DIRECT®
Engineering Structures 26 (2004) 781–799
ENGINEERING STRUCTURES
www.elsevier.com/locate/engstruct

Predicting the shear strength of reinforced concrete beams using artificial neural networks

M.Y. Mansour [a], M. Dicleli [b,*], J.Y. Lee [c], J. Zhang [a]

[a] Department of Civil Engineering, University of Brstish Columbia, Vancouver, BC Canada
[b] Department of Civil Engineering and Construction, Bradley University, 1501 West Bradley Avenue, Peoria, IL 61625-0114, USA
[c] Department of Architectural Engineering, Sungkyunkwan University, South Korea

Received 19 May 2003; received in revised form 17 September 2003; accepted 5 January 2004

Abstract

The application of artificial neural networks (ANNs) to predict the ultimate shear strengths of reinforced concrete (RC) beams with transverse reinforcements is investigated in this paper. An ANN model is built, trained and tested using the available test data of 176 RC beams collected from the technical literature. The data used in the ANN model are arranged in a format of nine input parameters that cover the cylinder concrete compressive strength, yield strength of the longitudinal and transverse reinforcing bars, the shear-span-to-effective-depth ratio, the span-to-effective-depth ratio, beam's cross-sectional dimensions, and the longitudinal and transverse reinforcement ratios. The ANN model was found to predict the ultimate shear stress well within the range of input parameters considered. The average value of the experimental shear strength to predicted shear strength ratios of the 176 specimens is 1.003. The ANN shear strength predicted results were also compared to those obtained using building codes' empirical equations and various-compatibility aided softened truss model theories. The results show that ANNs have strong potential as a feasible tool for predicting the ultimate shear strength of RC beams with transverse reinforcement within the range of input parameters considered. Finally, the ANN model was used to show that it could perform parametric studies to evaluate the effects of some of the inputs parameters on the chosen output.

Keywords: Artificial neural network; Shear strength; Reinforced concrete; Truss model; Building codes

1. Introduction

The behavior and design of reinforced concrete (RC) beams in shear remains an area of concern for structural engineers due to the sudden and brittle failure of RC beams dominated by shear action and due to the lack of rational design equations in building codes. The partial collapse of the Wilkins Air Force Depot warehouse in Ohio, in 1955, which was caused by shear failure of RC beams, raised concerns about the inadequate shear design practice at that time. Since then, design code procedures have evolved and become more stringent to prevent such sudden failures.

The shear failure modes, the resisting mechanisms at cracked stages, and the role of various parameters are presently under discussion and subject to debates among researchers. In addition, research studies [1–7] have been carried out with regard to the characteristic parameters that affect the shear strength of RC beams. Some of these parameters include material strength, shear-span-to-effective-depth ratio, amount of reinforcement as well as size and shape of the beam. The traditional approach used in most research in modeling the effect of these parameters on the shear strength of an RC beam starts with an assumed form of empirical or analytical equation and is followed by a regression analysis using experimental data to determine unknown coefficients, such that the equation will fit the test data. However, a comparative study of various models [4] for prediction of shear strength of RC beams has

* Corresponding author. Tel.: +1-309-677-3671; fax: +1-309-677-2867.
E-mail address: mdicleli@bradley.edu (M. Dicleli).

0141-0296/$ - see front matter © 2003 Elsevier Ltd. All rights reserved.
doi:10.1016/j.engstruct.2004.01.011

demonstrated that they are effective only for interpreting their own experimental results used for their calibration. This discrepancy may be attributed to the differences in the variables used and the details of the experiments.

Unfortunately, rational and easy-to-use types of equations are not yet available in design codes to accurately predict the shear strength of RC beams with transverse reinforcement. Therefore, the present study examines the feasibility of using artificial neural networks (ANNs) to predict the shear strength of RC beams with transverse reinforcement using available data from past experiments.

An ANN is by definition an interconnected network of processing elements that has the ability to be trained to map a given input into the desired output. Since the shear behavior of RC beams failing in shear is influenced by various complex parameters and the experimental data available are scattered, then ANNs may be used as an effective tool to predict the shear strengths of RC beams failing in shear.

In this study, the shear design equations, as given by the American, Canadian and the New Zealand building design codes [8–10] as well as three-compatibility aided softened truss model theories, namely the modified compression field theory [11] (MCFT), the rotating angle softened truss model [12] (RA-STM) and the fixed angle softened truss model [13] (FA-STM), are selected to calculate the shear strengths of 176 RC beams collected from the literature. The shear strengths of the same beams are also predicted using the ANN model. The experimental shear strength results for the 176 beams are then compared to the results predicted using the codes' equations, softened truss model theories and the ANN model to assess the efficiency of the ANN model. Finally, the ANN model is used to demonstrate that it could perform parametric studies to evaluate the effects of some of the input parameters on the chosen output (shear strength in this study).

2. Ultimate shear strength of RC beams

Although many rational truss model theories have been proposed over the past two decades, such as the MCFT [11] and the RA-STM [12], to predict the strength and deformation characteristics of shear elements, the formulation of rational shear design equations using these theories is very complex due to the presence of both known and unknown variables, which are mutually dependent. Therefore, most shear design equations are derived from the equilibrium conditions of the simple 45°-truss model theory proposed by Ritter and Morsch at the turn of the 20th century. These equations are in turn modified using statistical analysis to account for the effects of flexure and the longitudinal reinforcement ratio on the shear strength of RC beams and are adopted in most design codes, such as the ACI building code [8]. The equations simply estimate the shear strength of an RC beam as the superposition of shear strength due to concrete alone and shear reinforcement alone. However, the shear strength of RC beams predicted using these simple equations was found to be very conservative when compared to experimental observations. This was mainly because the equations were based on the assumption that no interaction between shear resisting mechanisms occurs which contradicts the findings of many researchers [3,4]. As a result, different rational truss model theories [11–13] were developed to predict the shear strengths and behavior of shear-dominant structures.

In the following subsections, first the experimental data for the shear strength of 176 RC beams collected from the literature are introduced. Then, the shear design equations, as given by the American, Canadian and the New Zealand building design codes [8–10] as well as three-compatibility aided softened truss model theories (MCFT [11], RA-STM [12] and FA-STM [13]) are discussed briefly.

2.1. Experimental data

The collected experimental data included 176 RC beams all having shear reinforcement [5–7,14–25]. The complete list of the data of the 176 RC beams is presented in Table A1 of the Appendix with the name and reference source of each specimen. The data cover the shear strengths of the specimens that are subjected to either one or two point loads acting symmetrically with respect to the centerline of the beam span. The beams have different support conditions simulating simple span, continuous span and fixed support conditions. During the collection stage, specimens that did not fail in shear were excluded from the database.

Based on the previous research studies, some of the important parameters that are thought to affect the shear strength of RC beams are listed below:

- shear-span (a);
- effective span of beam (L);
- effective depth (d) and size of beam;
- width of web (b_w);
- material strength of concrete, flexural (longitudinal) reinforcement and shear (transverse) reinforcement (f'_c, f_{yl}, f_{yt});
- reinforcement ratios of longitudinal steel and shear steel (ρ_l, ρ_t).

2.2. Shear strength using building codes

2.2.1. ACI building code

The shear provisions in the ACI building code [8], ACI 318-02, originated from the 1962 ACI-ASCE Committee on Shear and Diagonal Tension [26]. The committee proposed an equation for calculating the shear strength in beams without shear reinforcement as expressed below:

$$v_c = V_c/b_w d = \left(0.16\sqrt{f'_c} + 17.2\rho_w \frac{V_u d}{M_u}\right) \quad \text{(MPa)} \quad (1)$$

where b_w is the breadth of beam; d the effective depth of beam; f'_c the cylinder concrete strength of concrete; ρ_w the longitudinal tensile reinforcement ratio; V_u and M_u are the shear and moment at the critical section, respectively.

The formulation of the above equation followed a two-step procedure. In the first step, a basic analysis of the stresses at the flexural crack in the shear-span was performed to identify the significant parameters. The concrete strength, amount of longitudinal tensile reinforcement and the shear-span-to-depth ratio were found to be the most important parameters that affect the shear strength of the beams. In the second step, the existing test data of RC beams were analyzed statistically to establish the constants 0.16 and 17.2 as given by Eq. (1) above.

For beams with transverse reinforcement, the ACI building code [8] states that the nominal shear strength, v_n, of RC beams is composed of the concrete shear contribution, v_c and the transverse reinforcement contribution, v_s, as given below:

$$v_n = v_c + v_s \quad (2)$$

where v_c is presented in Eq. (1) and v_s is expressed as

$$v_s = A_v f_{yv}/b_w s = \rho_v f_{yv} \quad (3)$$

In the above equation A_v is the area of vertical shear reinforcement; f_{yv} the yield stress of stirrups, s the spacing of stirrups; and ρ_v is the shear reinforcement ratio. The ACI building code also states that the concrete shear contribution and the shear reinforcement contribution must not be taken greater than $0.3\sqrt{f'_c}$ and $0.66\sqrt{f'_c}$, respectively.

2.2.2. CSA (Canadian Standards Association) building code

Two approaches are identified in the Canadian building code [9] for shear design: the general method (A23.3 C1. 11.4) and the simplified method (A23.3 C1. 11.3). The general method is based on the MCFT [11] and will not be used in this study, as the shear strength prediction as given by the original formulation of the MCFT [11] is addressed separately. Thus, the simplified method is used to calculate the shear strengths of the considered RC beams. The simplified method is permitted for flexural members that are not subject to significant axial tension as is the case for all considered beams in this study.

Similar to the ACI building code [8], the shear strength of a RC beam as given by the simplified method is composed of the concrete shear contribution and the transverse reinforcement contribution as expressed in Eq. (2). In the Canadian building code [9], two equations for the concrete shear contribution, v_c, are given depending on the amount of transverse reinforcement and the effective depth (d) of the beam as expressed below:

$$v_c = \frac{V_c}{b_w d} = 0.2\sqrt{f'_c} \quad \text{when}$$

$$A_v \geq \frac{006\sqrt{f'_c} b_w s}{f_{yv}} \quad \text{or } d \leq 300 \text{ mm} \quad (4)$$

$$v_c = \frac{V_c}{b_w d} = \left(\frac{260}{1000 + d}\right)\sqrt{f'_c} \geq 0.1\sqrt{f'_c} \quad \text{when}$$

$$A_v < \frac{006\sqrt{f'_c} b_w s}{f_{yv}} \quad \text{and} \quad d > 300 \text{ mm} \quad (5)$$

The shear strength contribution of the transverse reinforcement, v_s, has the same form as that of the ACI building code [8] as given by Eq. (3).

2.2.3. New Zealand concrete structures design code

The New Zealand concrete structures design code [10] is applicable to members with concrete strength up to 100 MPa and not resisting earthquake forces. The nominal shear capacity of an RC beam with transverse reinforcement is expressed as

$$v_n = (0.07 + 10\rho_w)\sqrt{f'_c} + \rho_v f_{yv} \quad (6)$$

The concrete contribution term in Eq. (6) must be within the minimum and maximum limits of $0.08\sqrt{f'_c}$ and $0.2\sqrt{f'_c}$, respectively.

2.3. Shear strength using softened truss models: MCFT [11], RA-STM [12], and FA-STM [13]

Three-compatibility aided softened truss models, namely the MCFT [11], the RA-STM [12] and the FA-STM [13], are briefly presented and used in this paper to predict the ultimate shear strengths of the 176 RC beams reported in the literature. All three truss model theories assume the cracked reinforced concrete to be a continuous material (smeared crack concept) and satisfy equilibrium equations, compatibility equations, and the constitutive relationships of the materials. The main tensile flexural and the transverse reinforcements are assumed to be smeared over the cross-section of the RC beam in the longitudinal and transverse directions, respectively. Neither the compatibility and equilibrium

Table 1
Stress–strain curves of concrete and steel bars used in the MCFT [11], RA-STM [12], and FA-STM [13] theories

	MCFT	RA-STM	FA-STM
Compression stress–strain curve of concrete (ascending branch)	$\sigma_d^c = \nu f_c'\left[2\left(\frac{\varepsilon_d}{\nu\varepsilon_o}\right) - \left(\frac{\varepsilon_d}{\nu\varepsilon_o}\right)^2\right]$	$\sigma_d^c = \nu f_c'\left[2\left(\frac{\varepsilon_d}{\nu\varepsilon_o}\right) - \left(\frac{\varepsilon_d}{\nu\varepsilon_o}\right)^2\right]$	$\sigma_2^c = \nu f_c'\left[2\left(\frac{\varepsilon_2}{\nu\varepsilon_o}\right) - \left(\frac{\varepsilon_2}{\nu\varepsilon_o}\right)^2\right]$
	$\nu = \frac{1}{0.8+170\varepsilon_r} \le 1.0$	$\nu = \frac{5.8}{\sqrt{f_c'}}\frac{1}{\sqrt{1+400\varepsilon_r}}$	$\nu = \frac{5.8}{\sqrt{f_c'}}\frac{1}{\sqrt{1+400\varepsilon_1/\eta}}$; $\eta = \frac{\rho_t f_{yt}}{\rho_l f_{yl}}$
Tension stress–strain curves of concrete	$\sigma_r^c = E_c\varepsilon_r$ if $\varepsilon_r \le \varepsilon_{cr}$	$\sigma_r^c = E_c\varepsilon_r$ if $\varepsilon_r \le \varepsilon_{cr}$	$\sigma_1^c = E_c\varepsilon_1$ if $\varepsilon_1 \le \varepsilon_{cr}$
	$\sigma_r^c = \frac{f_{cr}}{1+\sqrt{500\varepsilon_r}}$ if $\varepsilon_r > \varepsilon_{cr}$	$\sigma_r^c = f_{cr}\left(\frac{\varepsilon_{cr}}{\varepsilon_r}\right)^{0.4}$ if $\varepsilon_r > \varepsilon_{cr}$	$\sigma_1^c = f_{cr}\left(\frac{\varepsilon_{cr}}{\varepsilon_1}\right)$ if $\varepsilon_1 > \varepsilon_{cr}$
Shear stress–strain curve of concrete (in MCFT-local)	$v_{cimax} = \frac{0.18\sqrt{f_c'}}{0.31+\frac{24w}{a+16}}$	N/A	$\tau_{21}^c = \frac{(\sigma_1^c-\sigma_2^c)}{2(\varepsilon_1-\varepsilon_2)}\gamma_{21}$ (Ref. 29)
Steel stress–strain curves	$f_s = E_s\varepsilon_s \le f_y - \frac{\sigma_r^c}{\rho}$	$f_s = E_s\varepsilon_s$ if $f_s \le f_y'$ $f_s = (0.91-2B)f_y + (0.02+0.25B)E_s\varepsilon_s$ if $f_s > f_y'$	$f_s = E_s\varepsilon_s$ if $f_s \le f_y'$ $f_s = (0.91-2B)f_y + (0.02+0.25B)E_s\varepsilon_s$ if $f_s > f_y'$

Note: r and d denote the directions of the principal tensile and compressive stresses in concrete, respectively. 1 and 2 denote the directions of the applied principal tensile and compressive stresses, respectively.

equations nor the solution procedures of the three considered truss model theories are reported in this paper but can be found elsewhere [11–13]. Only the constitutive relationships of the materials (concrete and steel) are presented in Table 1. The constitutive relationships of the materials as given in the RA-STM [12] and FA-STM [13] are based on the research findings of Belarbi and Hsu [27,28]. Following the solution procedures of each truss theory, three separate computer programs were developed and executed to calculate the ultimate shear strength of each of the 176 RC beams.

Both the MCFT [11] and the RA-STM [12] theories assume that the inclination of the principal compressive stress in concrete coincides with the inclination of the principal compressive strain. The main difference between both theories is that in the MCFT [11] a crack-check has to be provided to insure that the concrete tensile stresses can be transmitted across cracks which in turn causes the local stresses in the reinforcement to be increased at the crack locations giving rise to shear stresses at the crack surfaces. On the other hand, in the RA-STM [12] a new smeared stress–strain curve of steel bars embedded in concrete was proposed to take care of the crack-check presented in the MCFT.

Although the RA-STM [12] and MCFT [11] are two rational models to predict the shear response of reinforced concrete elements, they are incapable of deriving the well-known ''concrete contribution'' in shear resistance. In order to predict the so-called ''concrete contribution'', Pang and Hsu [13] proposed FA-STM [13]. In this model, the concrete struts are assumed to remain parallel to the initial cracks, the direction of which is determined from the principal applied stresses just prior to cracking. In the FA-STM [13], the concrete compression and tension stress–strain curves as well as the steel bars' stress–strain curves are assumed to be the same as those given in the RA-STM [12] with only minor modifications. Additionally, the concrete shear constitutive relationship is based on the one derived by Zhu et al. [29] and specified in Table 1.

3. Artificial neural networks (ANNs)

ANNs are, by definition, interconnected networks of processing elements that have the ability to be trained to map a given input into the desired output. ANNs possess some distinctive properties not found in conventional computational models. Traditional computing models are based on predefined rules (equations, formulas, etc.) that clearly specify the problem. The program follows an explicit step-by-step procedure to compute desired outputs. This is feasible when the rules defining the problem are known in advance. In most cases however, there are only observational data of the problem, while the underlying rules relating the input variables to the output variables are either unknown or extremely difficult to discover. Under there circumstances, ANNs exhibit their superiorities over conventional computational techniques.

ANNs are composed of many interconected processing units. Each processing unit keeps some information locally, is able to perform some simple computations, and can have many inputs but can send only one output. The ANNs have the capability to respond to input stimuli and produce the corresponding response, and to adapt to the changing environment by learning from experience. Therefore, in order for researchers to use ANNs as a predictive tool, data must be used to train and test the model to check its successfulness.

There are a number of ANN paradigms [30,31], but the most widely used are the multi-layer back-propagation neural networks (MBNNs). The MBNNs have been applied to solve many structural engineering applications as reported by many researchers [32–35] and are also employed in this research.

3.1. MBNN architecture

Generally, an MBNN is made of an input layer of neurons, sometimes referred to as nodes or processing units, one or several hidden layer of neurons and an output layer of neurons. The neighboring layers are fully interconnected by weights. The layout of the three-layer neural network used in this study is illustrated in Fig. 1(a). The network shown consists of an input layer with nine neurons, a hidden layer with three neurons, and an output layer with one neuron. The input layer neurons receive information from the outside environment and transmit them to the neurons of the hidden layer without performing any calculation. The hidden layer neurons then process the incoming information and extract useful features to reconstruct the mapping from the input space to the output space. Finally, the output layer neurons produce the network predictions to the outside world.

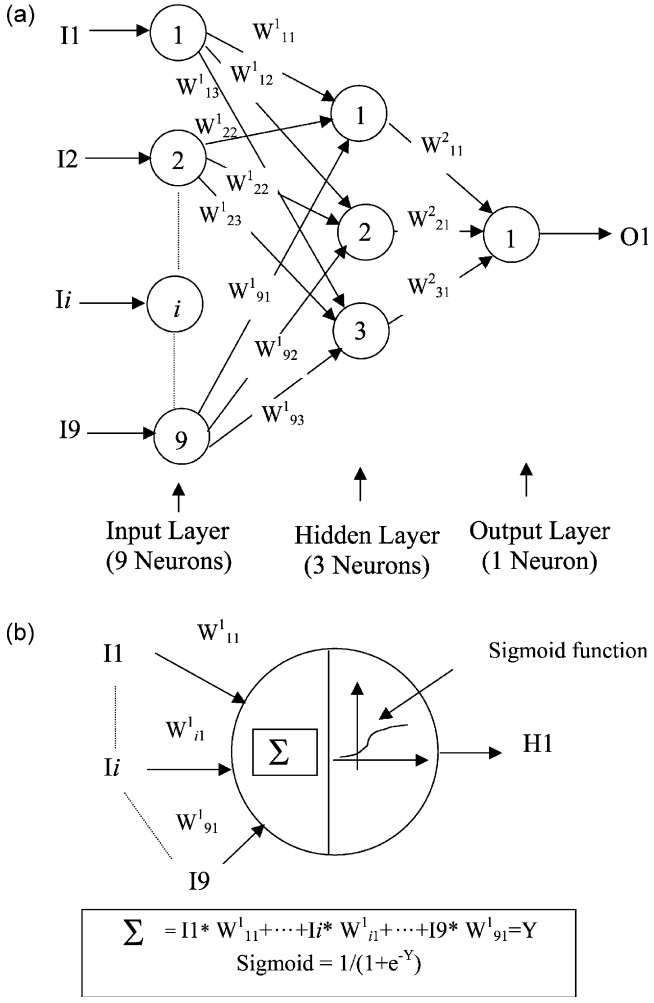

Fig. 1. Artificial neural network. (a) A typical MBNN, (b) typical neuron in a hidden layer.

Prior to being applied for prediction, the neural network architecture must be set up (the number of hidden layer and the number of neurons in each layer), then a set of training samples are used to train the network so that it learns the functional relationship between the input variables and the output variables. The amount of learning is proportional to the difference between the target output and the computed output. This learning process will in turn lead to adjusting the weights of the neurons to minimize the discrepancy between the two output values (target and computed) as explained in the next section.

At the start of the training, the weights are randomly set to arbitrary small real numbers. Then the examples are presented to the network and a forward pass operation is performed. Each neuron calculates the weighted sum of its inputs and transmits the result through a transfer function from which the neuron output is obtained. The data flow forward layer by layer. The discrepancies between the target and the predicted outputs measure the training error. In order to achieve satisfactory estimation, the weights of the network must be adapted to minimize the training error. This is done by a backward pass of the error, which is referred to as error back-propagation. The network error is passed backwards from the output layer to the input layer, and the weights are adjusted based on some learning strategies so as to reduce the network error to an acceptable level. One pass through the set of training inputs, together with the modification of the weights, constitutes one cycle or epoch. After the network is well trained, all the weights are frozen, and the network can then be applied for prediction within the domain covered by the inputs of the training examples.

The basic unit of a neural network is the neuron that determines the function of the entire network. A schematic diagram of an artificial neuron is illustrated in Fig. 1(b). The neurons receive inputs from the neurons of the preceding layers, calculate the weighted sum of the inputs and subtract a threshold value. Finally, the neurons pass this outcome through a transfer function producing the neurons outputs, which in turn are transmitted to the neurons of the next layers as inputs. Some examples of commonly used transfer functions are depicted in Fig. 2. In this study, the S-shaped sigmoid function is chosen and used to produce the

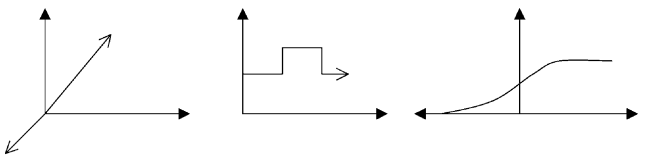

(a) Linear function (b) Step function (c) Sigmoid function

Fig. 2. Different types of transfer functions used in ANN.

neuron output. There are two important features of the sigmoid function. First, this transfer function introduces non-linearity that further enhances the neural network's ability to model complicated functions [36]. Second, because of the property of the sigmoid function, which is asymptotic to values 0 and 1, it produces very small signal error that will help in the network learning procedures.

To better explain the above-mentioned ANN procedure, the ANN network shown in Fig. 1(a) is taken as an example. The error "E" between the computed value (denoted by O_k) and the target output (denoted by T_k) of the output layer is defined as

$$E = \frac{1}{2}\sum_{k=1}^{n}(O_k - T_k)^2 \tag{7}$$

where

$$O_k = F(I_i W_i^k) = F\left(\sum_{i=1}^{3} I_i W_i^k\right) \tag{8}$$

In the equation above, $F(\ )$ is the sigmoid function defined in Fig. 1(b), I_i is the input to neuron "k" of the single output layer from neuron "i" of the hidden layer, and W_i^k is the weight associated between neuron "i" of the hidden layer and neuron "k" of the output layer. Note that in the ANN model shown in Fig. 1(a), only one output is used and thus the subscript "n" in Eq. (7) (summation sign) is equal to 1.

The learning mechanism of back-propagation networks is a generalized delta rule [31] that uses the gradient descent to minimize the error between the computed and the target output. Therefore, from the hidden layer to the output layer, the modification of weights is represented respectively by the following expression:

$$\Delta W_i^k = \lambda \delta_k I_i \tag{9}$$

where λ is the learning rate and $\delta_k = (T_k - O_k)$ $F'(I_i W_i^k)$. From the input layer to the hidden layer, similar equations can also be written

$$\Delta W_i^j = \lambda \delta_j I_i \tag{10}$$

where $\delta_j = W_{kj}\delta_k F'(I_i W_i^j)$.

The training algorithm can be improved by adding momentum terms into the weights equations as shown below:

$$W_i^k(t+1) = W_i^k(t) + \lambda\delta_k I_i + \gamma\left[W_i^k(t) - W_i^k(t-1)\right] \tag{11}$$

$$W_i^j(t+1) = W_i^j(t) + \lambda\delta_k I_i + \gamma\left[W_i^j(t) - W_i^j(t-1)\right] \tag{12}$$

where "t" denotes the learning cycle and "γ" is the momentum factor.

The process of forward and back-propagation continues until either the error is reduced to an acceptable target value or the program runs for a specified time. Although the back-propagation learning algorithm is widely used, this algorithm has a slow rate of learning [31]. Moreover, the convergence rate is highly dependent on the choice of the values of momentum and learning ratios accounted for in this algorithm. A detailed explanation of back-propagation networks is beyond the scope of this paper. However, the basic algorithm for back-propagation neural networks is described elsewhere [31,38].

4. ANN models used for the prediction of shear strength

4.1. ANN models and selection of input parameters

In this study, a computer program [37] based on the MBNN algorithm [38,39] with momentum is used in the simulations to develop an ANN model for predicting the ultimate shear strength of RC beams with stirrups. The program requires the following input data:

1. The error tolerance, which is set to 3% in this study, and is defined according to the root mean square error (RMSE).
2. The maximum number of training cycles or epochs, which is chosen as 50,000 to achieve the specified error tolerance. Once this number is attained the program is terminated even if the error tolerance is not met.
3. The total number of data that is presented (in this case, 176 RC beams were considered). The computer program uses 80% of the total data for training and the remaining 20% for testing.
4. The number of input neurons (nine in this study) and output neurons (one in this study).
5. A learning rate and a momentum factor, which are set equal to 0.4 and 0.2 in this study.

The following nine variables are used as input parameters for the ANN model constructed in this investigation: (1) f'_c; (2) f_{yl}; (3) f_{yt}; (4) a/d; (5) b_w; (6) d; (7) L/d; (8) ρ_l; (9) ρ_t. The output was selected as the ultimate shear strength ($V/b_w d$) of the RC beam. The ranges of the input parameters in the experimental database used are presented in Table 2.

ANN simulations are conducted using the program by experimentation. Values of the learning rate and momentum factor are varied while fixing the number of hidden layers and number of neurons in the hidden layers. In most of the simulations, it is found that one hidden layer and values of 0.4 for the learning rate and 0.2 for the momentum factor would lead to a minimum

Table 2
Ranges of input parameters in database

Input parameters	Range (min–max)
f'_c (MPa)	12.7–42.2
f_{yl} (MPa)	340–1029
f_{yt} (MPa)	250–1431
a/d	1.56–7.2
b_w (mm)	140–305
d (mm)	244–495.3
L/d	3.33–14.4
ρ_l (%)	0.61–4.76
ρ_t (%)	0.099–1.47

error. As far as the hidden layer is concerned, there is no general rule for selecting the number of neurons in a hidden layer. The choice of hidden layer size is mainly problem specific and to some extent depends on the number and quality of training patterns. The number of neurons in a hidden layer must be sufficient for the correct modeling of the problem, but it should be sufficiently low to insure generalization [40,41]. In this study, while designing the ANN model, it is found more appropriate to carry out a parametric study by changing the number of neurons in the hidden layer in order to test the stability of the network while keeping the values of the learning rate and momentum factor equal to 0.4 and 0.2, respectively. The performance of the network with various hidden neurons is measured by the RMSE, obtained during the training of each network. Accordingly, it was concluded that three neurons in the hidden layer result in a stable and optimum network leading to a minimum RMSE value.

4.2. Normalization of input and output data

Data scaling is an essential step for network training. One of the reasons for pre-processing the input and output data is the use of the sigmoid transfer function in this research. The sigmoid function constraints the output to lie within the range (0,1). Scaling of the inputs to the range (−1,+1) greatly improves the learning speed, as these values fall in the region of sigmoid transfer function where the output is most sensitive to variations of the input values. It is therefore recommended to normalize the input and output data before presenting them to the network. Various normalization or scaling strategies have been proposed [40,42]. In this study, a simple linear normalization function is used for the input parameters as shown below:

$$U = -1.0 + 2.0(X - X_l)/(X_u - X_l) \quad (13)$$

where U denotes the normalized value of input X; and X_l and X_u denote the lower and upper bounds of input variable X.

For the output parameters, usually a linear transformation works well, although a non-linear transformation is usually recommended if the data are clustered as is the case in this investigation. Thus, in this work, the output parameters are first transformed in the following:

$$S = \ln(Y) \quad (14)$$

where Y denotes the target value of output variable and ln denotes Napier logarithm. Then, S is normalized within the values of 0.1–0.9 for the sigmoid function as shown below:

$$V = 0.1 + 0.8(S - \ln Y_l)/(\ln Y_u - \ln Y_l) \quad (15)$$

where V denotes the normalized target value of ln (Y) or S; and Y_l and Y_u denotes the lower and upperbounds of the output variable Y, respectively.

4.3. Training and testing data

The experimental shear strength of the RC beam is used as the target value. The data of the 176 RC beams are grouped randomly into training set and testing set before presenting them to the network for analysis. Out of the 176 collected data, 140 are used for training the network and 36 are used to test the network. The ANN model was able to learn all the patterns presented with an RMSE error of less than 0.03 after 45,000 cycles of training.

5. Analysis results

5.1. Predicted results using ANN and other methods

The ANN model developed in this research is used to predict the shear strengths of the 176 RC specimens. The ratio of the experimental shear strength to the ANN predicted shear strength of each RC beam is given in Table A1. The average value of these ratios as given by ANN is 1.003 with a COV of 4%. The results of Table A1 indicate that the neural network was successful in learning the relationship between the different input parameters and the single output (shear strength). The results of the testing phase (shown in bold in Table A1) suggest that, although the model was not trained for these data, the neural network was capable of generalizing the relationship between the input variables and the output and yielded reasonably good predictions. The average value and COV of the experimental to predicted shear strength ratios of the data used to test the ANN are 1.01% and 5%, respectively.

The ANN shear strength results as well as those obtained from the ACI, CSA, New Zealand building design codes [8–10] and three-compatibility aided softened truss models (MCFT [11], RA-STM [12], and

FA-STM [13]) are shown in Fig. 3(a)–(g). Fig. 3(a)–(c) displays the predicted shear strengths versus the experimental shear strengths of the RC beams using the MCFT [11], RA-STM [12], and the FA-STM [13]. The predicted results using the MCFT [11] and the RA-STM [12] exhibit approximately the same trend for RC beams when the ultimate shear stress is less than 4 MPa. For larger values of the ultimate shear stress, the MCFT [11] shows more scatter when compared to the predicted results of the RA-STM [12]. However, in this range, both models tend to overestimate the ultimate shear stress. On the other hand, the predicted results of the FA-STM [13] tend to underestimate the actual shear strengths of the RC beams. The mean value and COV of the ratios of the experimental to predicted shear strength values for each method are also given in Fig. 3(a)–(g) and in Table 3 for comparison purposes.

The predicted results using the ACI [8] and CSA [9] building codes underestimate the observed shear strength of the RC beams as shown in Fig. 3(d) and (e), respectively, while the predicted shear strength results of the RC beams using the New Zealand concrete structures design code [10] (Fig. 3(f)) produces variations on either side of the desired ratio of 1. The New Zealand concrete structures design code tends to predict

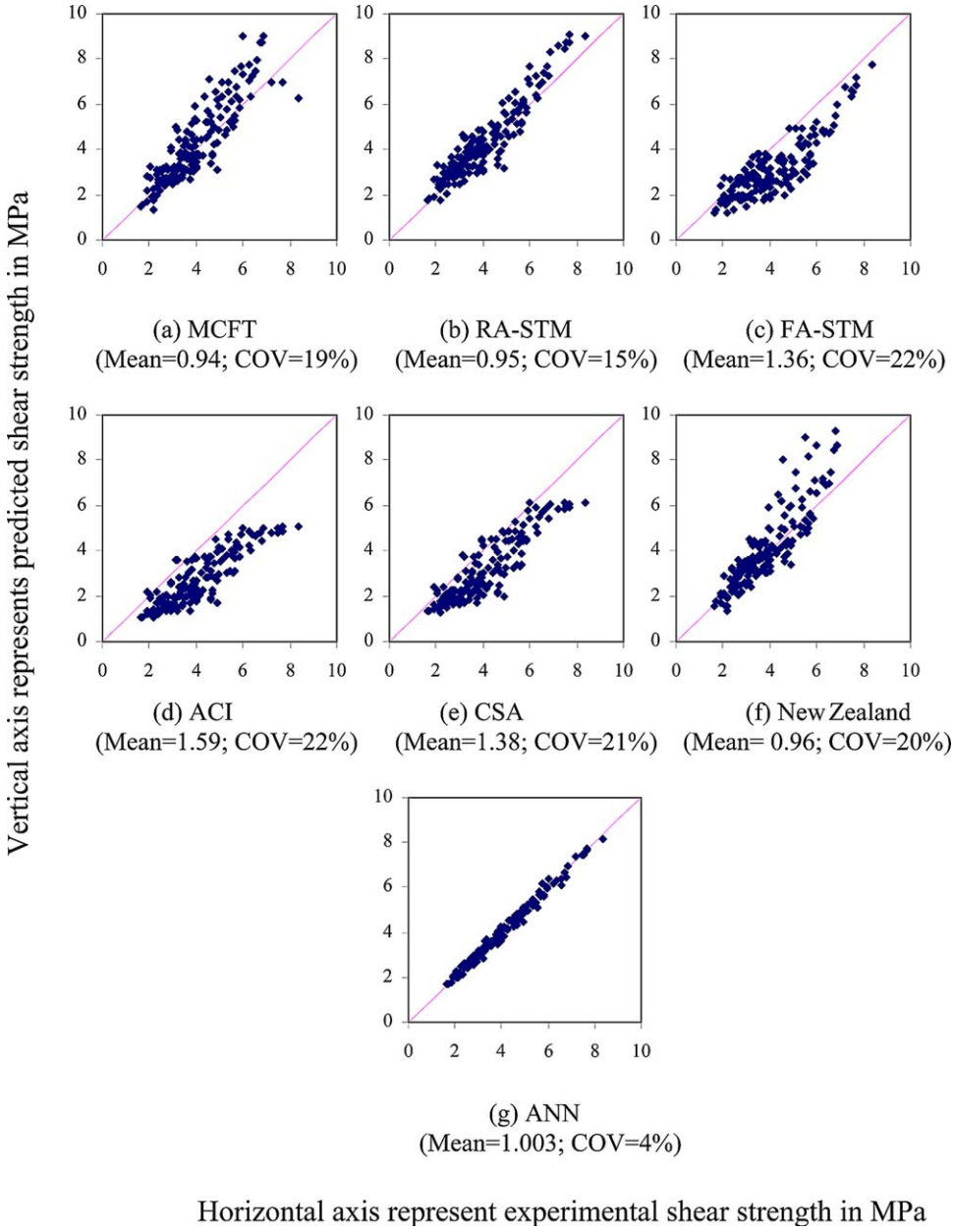

Fig. 3. Comparison of predicted shear strengths versus experimental shear strengths using various methods (*Note*: mean and COV values are based on the ratios of experimental to predicted shear strength values).

Table 3
Average and COV values of experimental to predicted shear strength values

Method used	Average value	COV (%)
MCFT	0.94	19
RA-STM	0.95	15
FA-STM	1.36	22
ACI	1.59	22
CSA	1.38	21
New Zealand	0.96	20
ANN (all data)	1.003	4
ANN (test data)	1.01	5

the shear strength better than those given by the ACI and CSA building codes [8,9].

The average value of the ratios of the experimental to predicted shear strength values of all RC beams is 0.947 in the MCFT [11], 0.952 in the RA-STM [12], 1.361 in the FA-STM [13], 1.597 in the ACI method [8], 1.386 in the CSA method [9], 0.96 in the New-Zealand method [10], and 1.003 in the ANN method. These values as well as Fig. 3(a)–(g) show clearly that the ANNs method can predict the shear strength of the RC beams much better than the other considered methods.

5.2. Effect of certain parameters on experimental to predicted shear strength ratio

In this section, the ACI [8], CSA [9], and the ANN methods as well as the three-compatibility softened truss model theories are considered to further investigate the effect of some of the variables on the predictions of the shear strengths of the RC beams. Although many important variables affect the shear behavior of RC beams, only the concrete strength, percentages of reinforcement in the longitudinal and transverse directions, the shear-span-to-depth ratio, as well as the depth-to-width ratio will be considered to assess the effects of these variables on the predicted shear strengths results.

5.2.1. Effect of concrete strength

The variation of the experimental shear strength to predicted shear strength ratio (referred to in this paper as the ultimate shear stress ratio) versus the concrete compressive strength for each method is shown in Fig. 4(a)–(f). From the figures it is clear that the ACI [8], CSA [9], and the FA-STM [13] methods yield conservative and scattered results for the range of concrete strength being investigated. The values of ultimate shear stress ratios using the RA-STM [12] and MCFT [11] display less scatter. Furthermore, the results obtained using the RA-STM exhibit less scatter when compared to those of the MCFT (COV of RA-STM [12] is 14% while that of MCFT [11] is 19%). This is because the softening coefficient of cracked concrete in compression proposed by Belarbi and Hsu [28] in the RA-STM [12] is a function of both the concrete cylinder compressive strength and the tensile strain, while that of the MCFT [11] does not include the effect of the concrete strength. The results of ultimate shear stress ratios using the ANN model indicate consistent accuracy for the range of concrete strength being investigated as shown in Fig. 5(f).

5.2.2. Effect of longitudinal and transverse reinforcement ratios

Fig. 5 displays the variation of the ultimate shear stress ratio as a function of the longitudinal reinforcement ratio for the three truss models, as well as the ACI [8], the CSA [9], and the ANN methods. The ultimate shear stress ratios using the MCFT [11] and the RA-STM [12] show less scatter when the longitudinal reinforcement ratio is within the range of 1–2.5%. This is because the constitutive relationships of the materials in both theories were calibrated for RC panels with amount of reinforcing steel falling within the above-mentioned range. On the other hand, the results as given by the FA-STM show more scatter when compared to those of the MCFT [11] and RA-STM [12] theories and tend to be very conservative when compared to the experimental observations (the values of the ultimate shear stress ratios are more than one). In addition, the results as given by the ACI and CSA building codes are also on the conservative side but show lots of scatter as the longitudinal reinforcement ratio increases. On the other hand, the ANN results are not affected by the variation in the longitudinal reinforcement ratios.

Fig. 6 displays the effect of the transverse reinforcement ratio on the ultimate shear stress ratio for the three truss models, as well as the ACI [8], the CSA [9], and the ANN methods. The ultimate shear stress ratios using MCFT [11] and RA-STM [12] show more scatter when the transverse reinforcement ratio is less than 0.5% (Fig. 6(a) and (b)). This trend is mainly due to the fact that the constitutive concrete relationships as proposed in both truss model theories are based on RC elements with transverse reinforcement ratios larger than 0.5%. The results of the FA-STM [13], ACI [8], and CSA [9] are found to be conservative within the range of transverse reinforcement ratio being investigated, while those of the ANN model are not affected by the change in transverse reinforcement ratio as shown in Fig. 6(c)–(f).

To further check the safety involved in the predicted results as given by the FA-STM compared to the predicted results as obtained by the MCFT [11] and RA-STM [12], the ultimate shear stress ratios for the MCFT [11], RA-STM [12], and FA-STM [13] are plotted against the ratios, μ, of the transverse to longitudinal

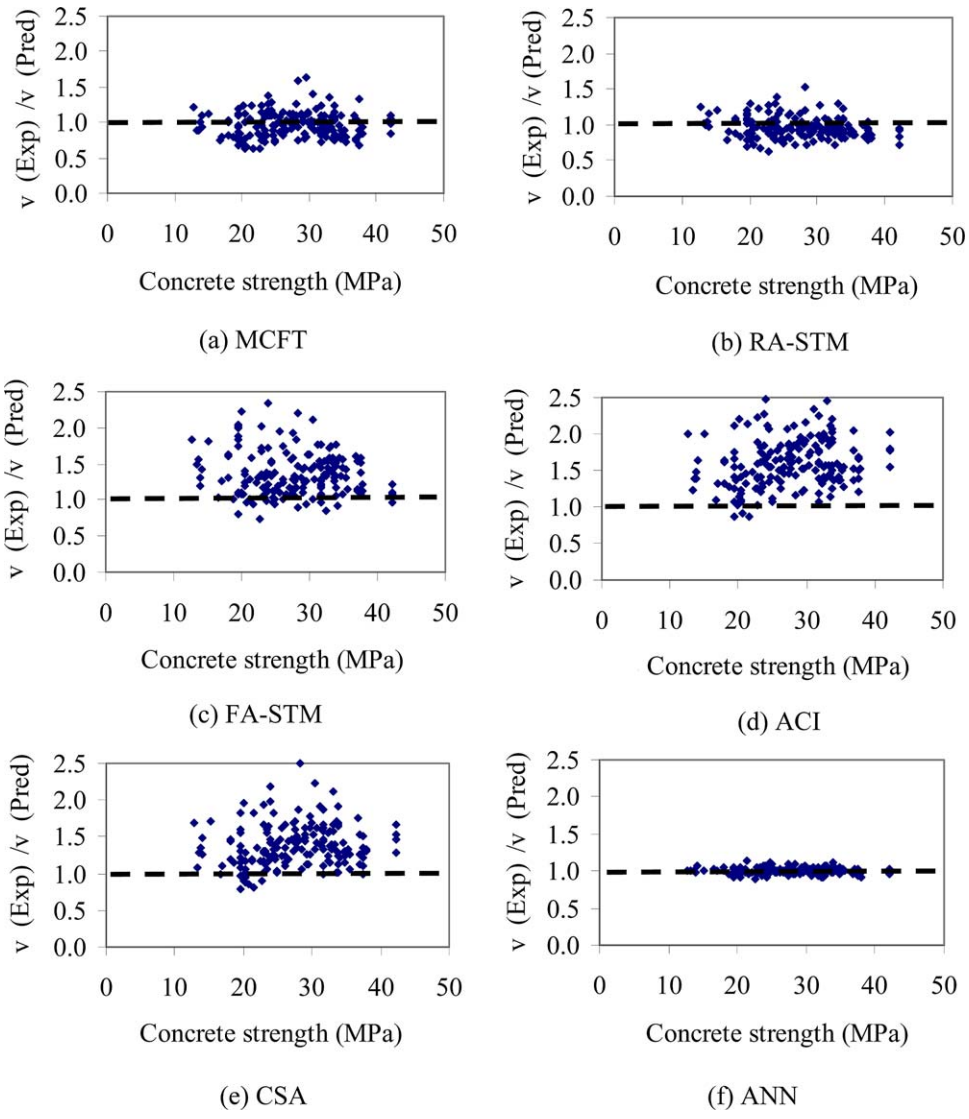

Fig. 4. Variation of experimental to predicted shear strength ratio with concrete strength (f'_c) using different methods.

reinforcing indexes for all RC beams, as shown in Fig. 8. This ratio is denoted by $\mu = \rho_t f_{yt}/\rho_l f_{yl}$. Fig. 7 clearly shows that the FA-STM results are conservative and exhibit lots of scatter for values of μ smaller than 0.25, unlike the results obtained using the MCFT [11] and RA-STM [12] theories. This threshold value of μ (0.25) was presented by Pang and Hsu [13] when proposing the range of applicability of their FA-STM theory for RC structures. This discrepancy between the predicted results and experimental results as given by the FA-STM [13] for values of μ less than 0.25 is explained by Lee et al. [22] and is mainly due to the excessive crack rotation in concrete as the difference between the longitudinal and transverse reinforcement ratios increases. For values of μ larger than 0.25, the ultimate shear stress ratio given by FA-STM [13] becomes closer to one.

5.2.3. Effect of shear-span-to-effective-depth ratio

The variations of the ultimate shear stress ratios with a/d values are shown in Fig. 8. Once again, the results obtained using the MCFT [11] and RA-STM [12] display less scatter than those obtained using the FA-STM [13], the ACI [8], and CSA [9] methods which lead to large variations with all values of a/d being investigated. On the other hand, results obtained from the ANN model show consistency and accuracy for all values of a/d being investigated.

5.2.4. Effect of depth-to-width ratio

The effect of the beam's size on the predicted results is presented in Fig. 9 In the figure, the size effect is represented by the ratio of the beam's depth to the web's width (d/b_w). As expected, the ANN predicted results are in reasonably good agreement for all ratios

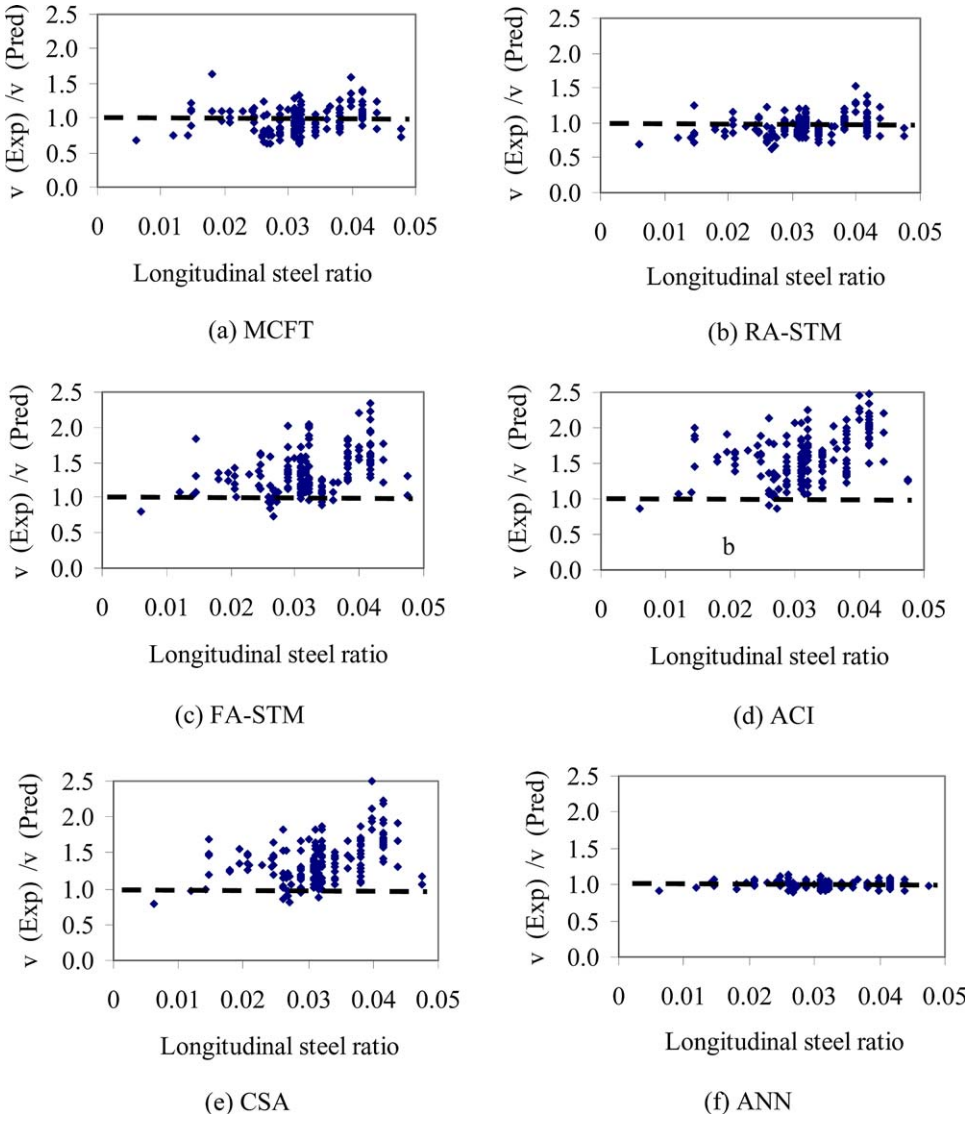

Fig. 5. Variation of experimental to predicted shear strength ratio with longitudinal steel ratio using different methods.

of d/b_w considered in this investigation. While the ACI, CSA, and FA-STM show lots of scatter and conservatism for all values of d/b_w, the predicted results as given by the RA-STM and the MCFT show less scatter and in some cases these two truss theories give predicted shear strengths larger than the experimental ones especially when the depth-to-web-width ratio is less than 3.

5.3. Parametric studies using ANN

Since the ANN model is found to be capable of generalization within the range of the input parameters being investigated, parametric studies are carried out in this section to evaluate the effects of some of the input parameters on the output. This is done by testing the model with hypothetical data by varying the values of some input parameters. In this section, two parametric studies are carried out as outlined below.

The first parametric study considers the effect of varying the shear-span-to-effective depth ratio and concrete strength on the ultimate shear strength of RC beams as shown in Fig. 10. This parametric study is carried out by changing the values of the a/d ratio and concrete strength (f'_c) while keeping the other input parameters constant as given below:

$d = 244$ mm; $b = 220$ mm; $\rho_l = 3.6\%$; $\rho_t = 0.22\%$; $f_{ly} = 402$ MPa; $f_{ty} = 358$ MPa; $L/d = 5$.

Fig. 10 shows that the ultimate shear strength of an RC beam increases with increasing concrete strength and decreasing a/d ratio. The results are in good agreement with findings of other researchers [4,5,14].

The second parametric study is carried out to show the variation of the ultimate shear stress of RC beams as a function of the longitudinal and transverse

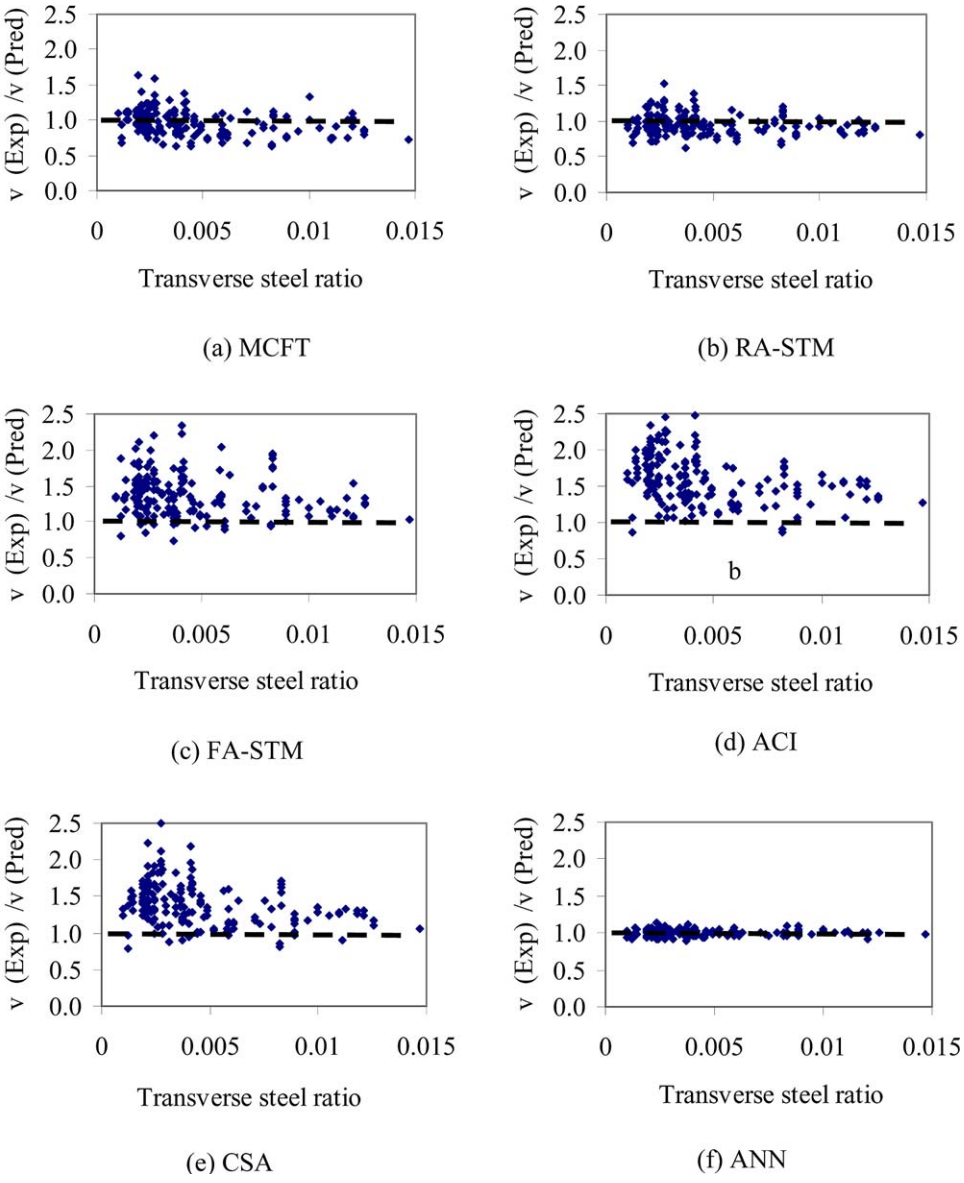

Fig. 6. Variation of experimental to predicted shear strength ratio with transverse steel ratio using different methods.

reinforcement ratios. In this parametric study, the values of the longitudinal and transverse reinforcement ratios are varied while keeping the other input parameters constant as shown below:

$d = 380$ mm; $b = 200$ mm; $a/d = 3.0$; $f'_c = 40$ MPa; $f_{ly} = 402$ MPa; $f_{ty} = 358$ MPa; $L/d = 5$.

The results of this second parametric study are presented in Fig. 11. To check the successfulness of this ANN parametric study, Fig. 11 also depicts the results as obtained by Zsutty's formula [43] given below:

$$v_u = 2.2\left(f'_c \rho \frac{d}{a}\right)^{1/3} + \rho_v f_{yv} \quad (16)$$

where the first term on the right-hand side needs to be multiplied by $2.5d/a$ when a/d is less than 2.5. The figure shows that the ANN parametric results and those of Zsutty's equation [43] show the same trend: the shear strength increases as the amount of longitudinal reinforcement or transverse reinforcement increases.

6. Use of ANN in structural engineering

The success of the ANN model in predicting the shear strengths of RC beams and in modeling physical processes highlights that such a numerical technique can be used reliably to produce ample shear strengths data of RC beams, within the range of input parameters used to train the model, rather than referring to

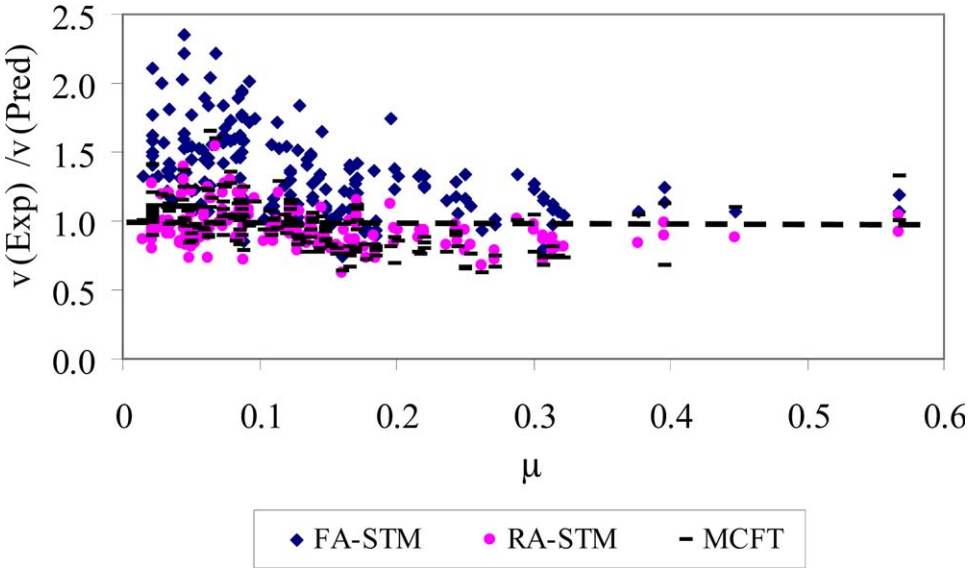

Fig. 7. Variation of ultimate shear stress ratio with μ as given by MCFT, RA-STM, and FA-STM.

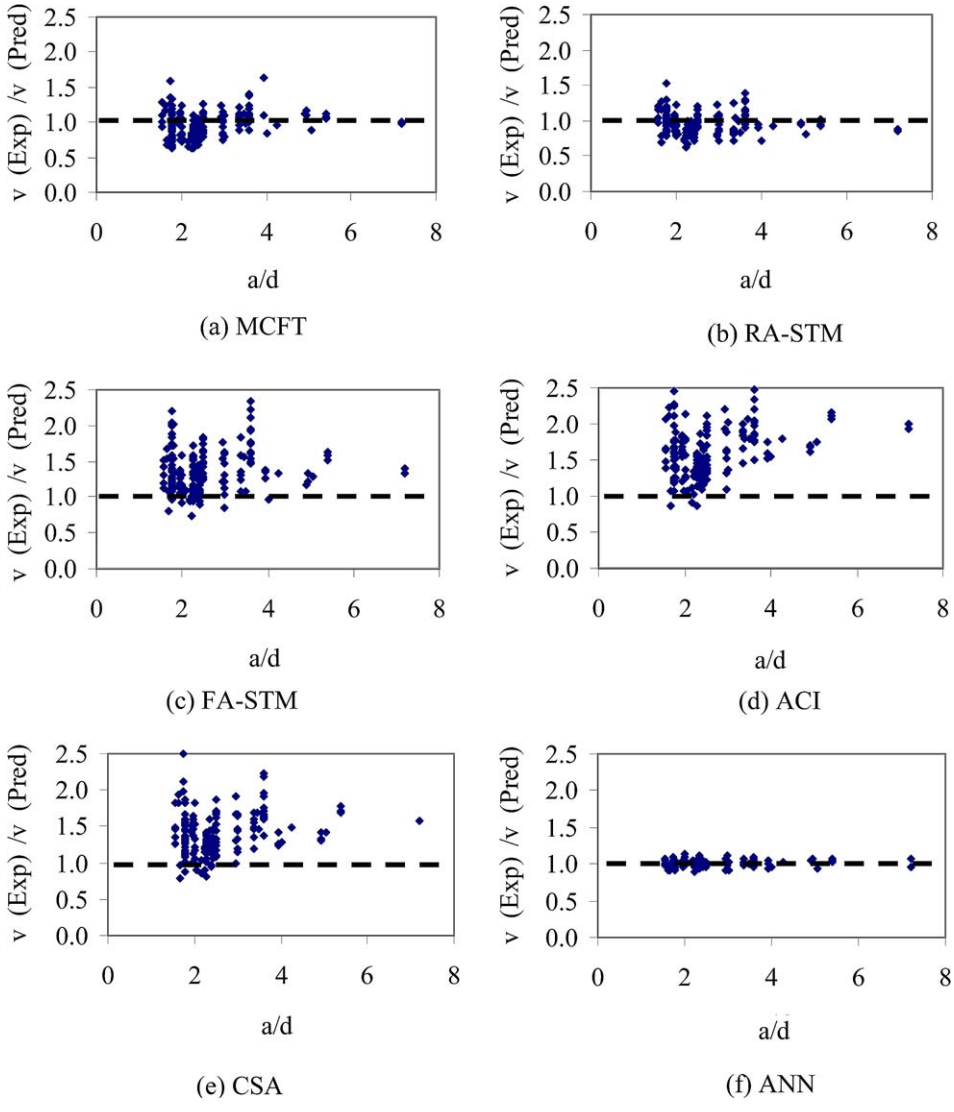

Fig. 8. Variation of experimental to predicted shear strength ratio with shear-span-to-effective-depth ratio (a/d) using different methods.

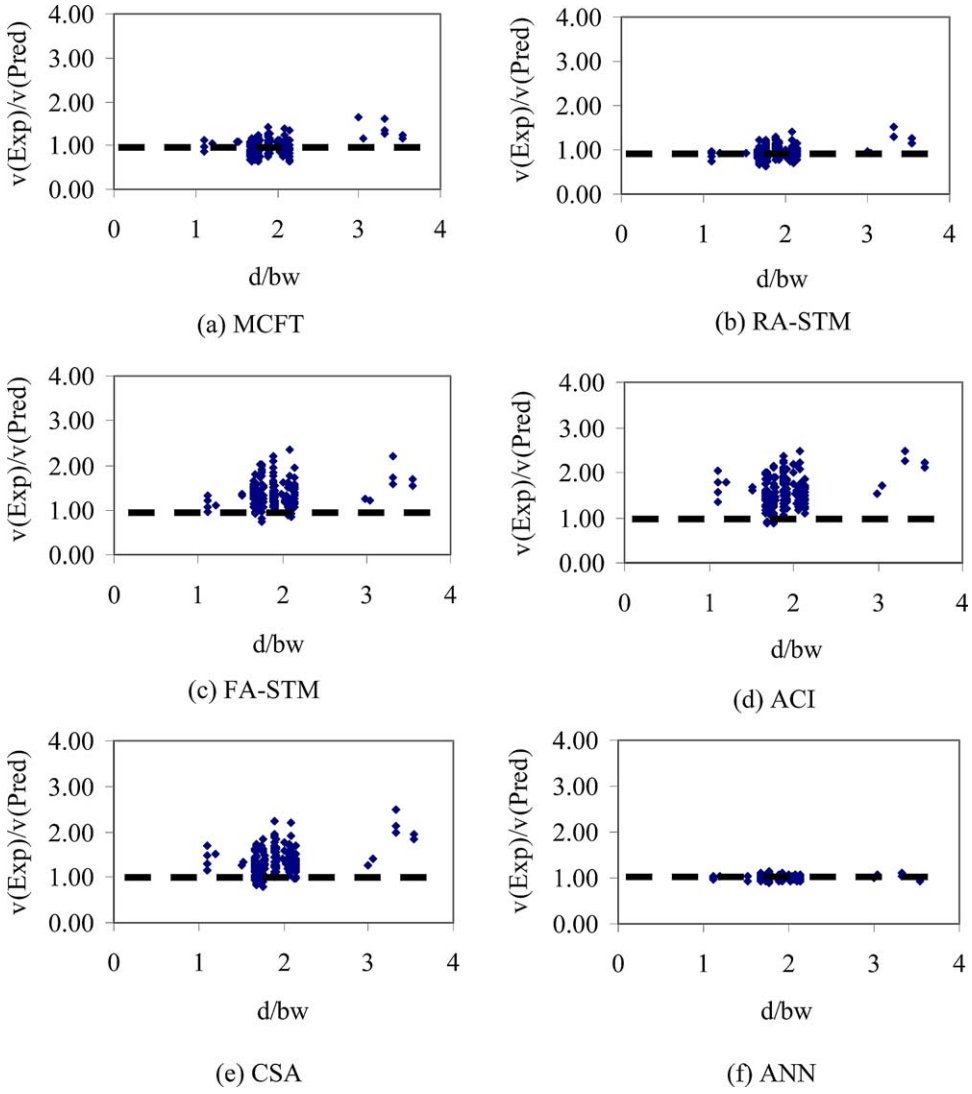

Fig. 9. Variation of experimental to predicted shear strength ratio with effective depth to web width ratio (d/b_w) using different methods.

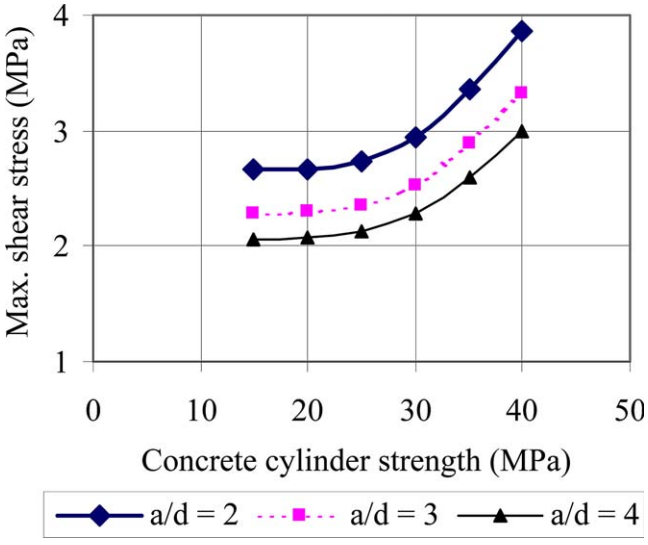

Fig. 10. Variation of maximum shear stress with concrete strength and a/d ratio as predicted by ANN.

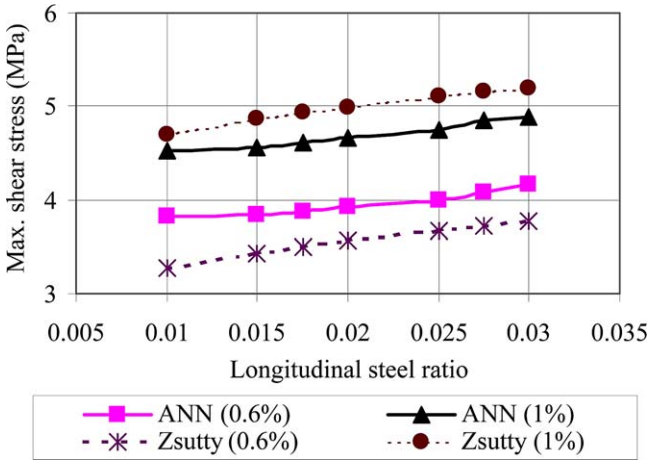

Fig. 11. Variation of maximum shear stress with longitudinal and transverse steel ratios (*Note*: value in bracket denotes the transverse steel ratio).

costly experimental investigation. The generated data can in turn be used to help propose and formulate mathematical equations that will help practicing structural engineers to predict more accurately the shear strengths of RC beams.

On the other hand, although ANN has been widely used in financial and electrical engineering practical problems [38,40], its use in structural engineering is still limited to research related problems only [41]. However, many easy-to-use software, such as the Propagator Software [44] and Predict Software [45] to name a few, that requires limited knowledge of ANN are now available and have been successfully used by researchers in structural engineering applications [34]. These simple software will hopefully encourage structural engineers to use such a numerical technique in practice in the near future. For instance, the Predict Software [45] is fully automated, and it selects parameters from a general list of input parameters. This software is compatible with MS Excel that facilitates the input of data.

7. Conclusions

The study conducted in this paper shows the feasibility of using a simple MBNN to predict the ultimate shear strengths of RC beams with transverse reinforcements. After learning from a set of selected training data, involving the shear strengths of transversely reinforced RC beams collected from the technical literature, the ANN model is used to successfully predict the shear strengths of the test data within the range of input parameters being investigated. Applying the ANN model to predict the shear strengths of RC beams with input parameters outside the range over which the model was trained does not guarantee adequate strength predictions. In such a case, more data should be collected to increase the range of input parameters needed to cover the domain of interest.

It is found that the strength values obtained from the ANN are more accurate than those obtained from design codes' empirical equations and sophisticated softened truss model theories. The average value of the ratios of the experimental shear strengths to predicted shear strengths is 0.947 in the MCFT [11], 0.952 in the RA-STM [12], 1.36 in the FA-STM [13], 1.597 in the ACI method [8], 1.386 in the CSA method [9], 0.96 in the New Zealand method [10], and 1.003 in the ANN model. The results also indicate that with proper training, ANN can provide an alternative method for predicting the strength capacities of structural members especially in cases where it is difficult to model the complex interactions among the multiple variables.

The effect of the concrete strength, the amount of steel in the longitudinal and transverse directions, the shear-span-to-effective-depth ratio, as well as the size of the beams on the predicted shear strength results as given by the ACI [8] and CSA [9] building codes, the three truss model theories, and the ANN was also studied. The study showed that within the range of input parameters being investigated, the results of the ANN show consistency and accuracy when compared to the results as given by other methods. Other methods showed scatter in the predicted results for different values of input parameters considered.

The ANN model was also used to perform parametric studies and was successful in modeling physical processes. The conducted parametric studies show that the shear strength of an RC beam increases as: (a) the concrete strength increases and the shear-span-to-depth-ratio decreases; and as (b) the amounts of longitudinal and transverse reinforcement increase. The results of the parametric studies were found to be in agreement with other research findings [3,5,14,43].

Appendix A.

Table A1
Data and ratios of experimental shear strength to predicted ANN shear strength of beams

Beam	b (mm)	d (mm)	F'_c (MP_a)	f_{dy} (MP_a)	f_{ty} (MP_a)	a/d	ρ(long.) (%)	ρ(tran.) (%)	L/d	v_{u-Exp} (MP_a)	$V_{u-exp/w-ANN}$	Ref.
A-1	307	466	24	555	325	3.94	1.80	0.10	7.8	1.63	0.942	25
A-2	305	464	24	555	325	4.93	2.28	0.10	9.9	1.73	1.035	25
B-1	231	461	25	555	325	3.94	2.43	0.15	7.9	2.09	1.051	25
B-2	229	466	23	555	325	4.91	2.43	0.15	9.8	1.88	1.040	25
C-1	155	464	30	555	325	3.94	1.80	0.20	7.9	2.17	1.007	25
C-2	152	464	24	555	325	4.93	3.66	0.20	9.8	2.30	1.080	25
A1-1	203	390	25	321	331	2.35	3.10	0.38	4.7	2.80	1.106	15

(continued on next page)

Table A1 (*continued*)

Beam	b (mm)	d (mm)	F'_c (MP_a)	f_{dy} (MP_a)	f_{ty} (MP_a)	a/d	ρ(long.) (%)	ρ(tran.) (%)	L/d	v_{u-Exp} (MP_a)	$V_{u-exp}/w-_{ANN}$	Ref.
A1-2	203	390	24	321	331	2.35	3.10	0.38	4.7	2.64	0.933	15
A1-3	203	390	23	321	331	2.35	3.10	0.38	4.7	2.81	0.955	15
A1-4	203	390	25	321	331	2.35	3.10	0.38	4.7	3.08	0.987	15
B1-1	203	390	23	321	331	1.95	3.10	0.37	4.7	3.51	1.041	15
B1-2	203	390	25	321	331	1.95	3.10	0.37	4.7	3.23	0.982	15
B1-3	203	390	24	321	331	1.95	3.10	0.37	4.7	3.59	1.050	15
B1-4	203	390	23	321	331	1.95	3.10	0.37	4.7	3.37	1.021	15
B1-5	203	390	25	321	331	1.95	3.10	0.37	4.7	3.04	0.960	15
B2-1	203	390	23	321	331	1.95	3.10	0.73	4.7	3.80	0.977	15
C1-3	203	390	24	321	331	1.56	2.07	0.34	4.7	3.10	1.042	15
C3-1	203	390	14	321	331	1.56	2.07	0.34	4.7	2.82	1.062	15
C3-2	203	390	14	321	331	1.56	2.07	0.34	4.7	2.53	1.005	15
C3-3	203	390	14	321	331	1.56	2.07	0.34	4.7	2.37	0.974	15
C4-1	203	390	24	321	331	1.56	3.10	0.34	4.7	3.90	1.072	15
D1-6	152	315	28	321	331	1.94	3.42	0.46	7.8	3.65	1.002	15
D1-7	152	315	28	321	331	1.94	3.42	0.46	7.8	3.74	1.013	15
D1-8	152	315	28	321	331	1.94	3.42	0.46	7.8	3.88	1.032	15
D2-6	152	315	30	321	331	2.43	3.42	0.61	9.7	3.52	0.986	15
D2-7	152	315	28	321	331	2.43	3.42	0.61	9.7	3.28	0.957	15
D2-8	152	315	26	321	331	2.43	3.42	0.61	9.7	3.51	0.990	15
D4-1	152	315	27	321	331	2.43	3.42	0.49	9.7	3.51	1.019	15
D4-2	152	315	26	321	331	2.43	3.42	0.49	9.7	3.28	0.985	15
D4-3	152	315	22	321	331	2.43	3.42	0.49	9.7	3.45	0.992	15
D5-1	152	315	28	321	331	2.43	3.42	0.37	9.7	3.05	0.982	15
D5-2	152	315	29	321	331	2.43	3.42	0.37	9.7	3.28	1.012	15
D5-3	152	315	27	321	331	2.43	3.42	0.37	9.7	3.28	1.019	15
C205D10(1)	150	315	29	361	355	2.00	2.61	0.24	6.0	2.91	1.032	16
C205D20(2)	150	315	30	387	355	2.00	2.08	0.24	6.0	2.59	0.978	16
C210DOA(3)	150	315	34	361	355	2.00	2.61	0.47	6.0	3.45	1.005	16
C305DO(5)	150	315	33	361	355	3.00	2.61	0.24	6.0	2.28	0.923	16
1-V1/4(1)	140	464	24	329	378	1.75	3.99	0.27	5.3	3.99	1.045	17
2-V1/4(2)	140	464	33	329	378	1.75	3.99	0.27	5.3	4.62	1.023	17
2-V3/8(8)	140	464	28	329	329	1.75	3.99	0.27	5.3	4.91	1.091	17
1a-V1/4(13)	140	495	24	329	316	1.64	3.99	0.27	4.9	3.39	0.924	17
1a-V3/8(14)	140	495	23	329	357	1.64	3.99	0.27	4.9	3.75	0.990	17
R8	152	272	27	618	269	3.36	1.46	0.21	6.7	1.92	0.984	5
R11	152	272	26	618	269	3.36	1.95	0.21	6.7	2.16	1.020	5
R12	152	254	34	618	269	3.60	4.16	0.21	7.2	2.83	0.993	5
R14	152	272	29	618	269	3.36	1.46	0.14	6.7	2.16	1.015	5
R15	152	254	30	618	279	3.60	4.16	0.41	7.2	3.61	0.993	5
R16	152	254	31	618	279	3.60	416	0.41	7.2	361	0.992	5
R24	152	254	31	618	269	5.05	4.16	0.21	10.1	2.38	0.933	5
R25	152	254	31	618	269	3.60	4.16	0.21	7.2	2.70	0.976	5
R28	152	254	31	618	269	3.60	4.16	0.83	7.2	4.63	0.970	5
C4S2.0	220	264	42	402	358	2.00	2.67	0.32	4.0	3.75	1.020	14
C4S3.0	220	244	42	402	358	3.00	3.60	0.22	6.0	3.47	1.019	14
C4S3.5	220	244	42	402	358	3.50	3.60	0.22	7.0	3.05	0.997	14
C4S4.0	220	244	42	436	358	4.00	3.60	0.22	8.0	2.65	0.959	14
IA-2R(17)	178	306	18	602	526	2.99	2.47	0.24	6.0	4.64	0.993	18
IC-2R(19)	178	310	34	576	526	2.95	4.38	0.24	5.9	5.11	0.978	18
ID-2R(20)	178	306	34	602	526	2.99	2.47	0.24	6.0	3.94	0.924	18
A2	178	381	29	515	357	2.50	3.81	0.19	5.0	4.57	0.955	6
A3	178	381	30	515	343	2.50	3.81	0.42	5.0	5.26	0.995	6
A4	178	381	28	515	343	2.50	3.81	0.79	5.0	5.82	1.038	6
A5	178	381	26	515	343	2.50	3.81	1.26	5.0	4.94	0.990	6
B3	178	381	28	515	343	3.38	3.81	0.42	6.8	5.69	1.005	6
C2	178	381	28	515	357	4.25	3.81	0.19	8.5	5.98	1.002	6
E3	178	381	14	515	343	2.50	3.81	0.42	5.0	7.52	0.998	6
E4	178	381	13	515	343	2.50	3.81	0.79	5.0	8.33	1.025	6
E5	178	381	17	515	343	2.50	3.81	1.26	5.0	3.82	0.940	6
G3	178	381	26	515	454	2.50	3.81	0.42	5.0	5.73	0.925	6
G4	178	381	27	515	454	2.50	3.81	0.63	5.0	3.54	0.971	6

Table A1 (*continued*)

Beam	b (mm)	d (mm)	F'_c (MP_a)	f_{dy} (MP_a)	f_{ty} (MP_a)	a/d	ρ(long.) (%)	ρ(tran.) (%)	L/d	v_{u-Exp} (MP_a)	$V_{u-exp}/w-_{ANN}$	Ref.
G5	178	381	26	515	454	2.50	3.81	1.05	5.0	5.83	1.032	6
H2	178	381	28	515	343	2.50	3.81	0.42	5.0	3.94	1.000	6
T4	152	272	32	618	269	3.36	1.95	0.21	6.7	3.90	0.989	5
T6	152	254	26	618	269	3.60	4.16	0.83	7.2	5.36	0.984	5
T7	152	264	27	618	269	3.46	3.00	0.21	6.9	5.94	0.990	5
T8	152	254	31	618	269	3.60	4.16	0.21	7.2	6.57	1.027	5
T9	152	254	20	618	279	3.60	4.16	0.41	7.2	7.50	1.011	5
T10	152	272	28	618	269	3.36	1.46	0.14	6.7	7.21	0.977	5
T11	152	254	37	618	279	3.60	4.16	0.41	7.2	4.60	1.031	5
T12	152	254	31	618	269	3.60	4.16	0.21	7.2	5.49	1.055	5
T13	152	272	13	618	269	3.36	1.46	0.21	6.7	6.74	1.014	5
T14	152	254	33	618	269	3.60	4.16	0.83	7.2	7.68	0.995	5
T15	152	254	33	618	269	7.20	4.16	0.21	14.4	4.43	0.970	5
T16	152	254	33	618	269	7.20	4.16	0.14	14.4	4.00	1.007	5
T19	152	254	30	618	269	5.40	4.16	0.21	10.8	6.24	1.017	5
T32	152	254	28	618	269	3.60	4.16	0.83	7.2	7.55	1.010	5
T34	152	254	34	618	269	5.40	4.16	0.21	10.8	4.03	0.971	5
T35	152	254	34	618	269	5.40	4.16	0.21	10.8	4.33	0.955	5
T36	152	254	24	618	279	3.60	4.16	0.41	7.2	5.51	1.031	5
T37	152	254	32	618	269	3.60	4.16	0.83	7.2	4.97	1.020	5
IA-2(2)	178	306	18	602	526	2.99	2.47	0.24	6.0	6.55	1.068	18
IC-2(5)	178	310	34	576	526	2.95	4.38	0.24	5.9	6.79	1.057	18
IIA-2(9)	178	306	18	602	526	2.99	2.47	0.24	6.0	3.78	1.051	18
IIB-2(10)	178	308	17	581	526	2.97	1.41	0.24	5.9	4.77	1.041	18
IIC-2(12)	178	310	38	576	526	2.96	4.38	0.24	5.9	4.90	0.961	18
IID-2(13)	178	306	38	602	526	2.99	2.47	0.24	6.0	5.62	0.970	18
J3	178	381	30	515	343	2.50	3.81	0.42	5.0	6.30	1.012	6
J5	178	381	32	515	343	2.50	3.81	1.26	5.0	3.85	1.036	6
C205-S0(30)	150	315	21	358	353	2.00	2.61	0.24	4.0	6.87	0.988	6
IV-n(333)	178	305	23	312	314	2.00	4.76	0.95	4.0	7.66	1.002	7
IV-o(34)	178	305	24	312	327	2.00	4.76	1.47	4.0	3.43	1.001	7
B-210-6.0	180	340	20	798	1333	1.76	3.16	0.31	3.5	3.04	0.944	16
B-210-7.4	180	340	20	798	1422	1.76	3.16	0.44	3.5	4.81	0.978	19
B-210-9.5	180	340	20	798	1402	1.76	3.16	0.71	3.5	5.35	1.031	19
B-210-11.0	180	340	20	798	1431	1.76	3.16	1.00	3.5	4.01	0.965	19
B-360-4.1	180	340	38	798	1392	1.76	3.16	0.15	3.5	4.01	0.965	19
B-360-5.1	180	340	38	798	1422	1.76	3.16	0.23	3.5	4.41	0.966	19
B-360-6.0	180	340	38	798	1333	1.76	3.16	0.31	3.5	5.29	0.991	19
B-360-7.4	180	340	38	798	1422	1.76	3.16	0.44	3.5	4.49	1.055	19
B-360-7.4	180	340	38	798	1422	1.76	3.16	0.44	3.5	4.49	1.055	19
B-360-9.2	180	340	38	798	1402	1.76	3.16	0.71	3.5	2.40	0.927	19
B-360-11.0	180	340	38	798	1431	1.76	3.16	1.00	3.5	3.04	1.010	19
B-30-046	200	352	33	931	349	2.27	3.09	0.46	4.5	3.34	0.947	20
B-30-121	200	352	32	931	285	2.27	3.09	1.21	4.5	4.24	1.030	20
B-60-030	200	352	33	931	492	2.27	3.09	0.30	4.5	4.49	1.021	20
B-80-059	200	352	33	931	554	2.27	3.09	0.59	4.5	5.12	1.038	20
B-80-019	200	352	33	931	866	2.27	3.09	0.19	4.5	2.96	0.981	20
B-80-022S	200	352	34	931	824	2.27	3.09	0.22	4.5	4.01	0.958	20
B-80-046	200	352	34	931	901	2.27	3.09	0.46	4.5	4.73	0.983	20
B-80-058S	200	352	34	931	841	2.27	3.09	0.58	4.5	2.34	0.950	20
B-80-059	200	352	34	931	901	2.27	3.09	0.59	4.5	1.89	0.917	20
B-80-110S	200	352	34	931	803	2.27	3.09	1.10	4.5	3.22	1.129	20
B-80-121	200	352	34	931	898	2.27	3.09	1.21	4.5	3.82	1.104	20
B-120-019	200	352	35	931	1062	2.27	3.09	0.19	4.5	3.94	1.016	20
B-120-030	200	352	35	931	1062	2.27	3.09	0.30	4.5	3.63	1.014	20
B-120-059	200	352	35	931	1061	2.27	3.09	0.59	4.5	2.69	1.028	20
B-120-121	200	352	35	931	1066	2.27	3.09	1.21	4.5	2.46	0.950	20
B-150-019	200	352	35	931	1235	2.27	3.09	0.19	4.5	2.67	0.992	20
B-1.5-022	200	352	35	931	824	2.27	3.09	0.22	4.5	2.05	0.897	20
B-1.5-0583	200	352	35	931	841	2.27	3.09	0.58	4.5	2.58	0.979	20
B-1.5-110	200	352	36	931	803	2.27	3.09	1.10	4.5	3.21	1.012	20

(continued on next page)

Table A1 (*continued*)

Beam	b (mm)	d (mm)	F'_c (MP_a)	f_{dy} (MP_a)	f_{ty} (MP_a)	a/d	ρ(long.) (%)	ρ(tran.) (%)	L/d	v_{u-Exp} (MP_a)	$V_{u-exp}/w-_{ANN}$	Ref.
S10-M-2.0-21-40-1	200	336	20	854	830	2.38	2.88	0.40	4.8	2.91	0.972	21
S10-M-2.0-21-59-1	200	336	20	854	830	2.38	2.88	0.59	4.8	3.13	0.966	21
S10-M-2.0-21-89-1	200	336	21	854	830	2.38	2.88	0.89	4.8	2.93	1.042	21
S10-M-2.0-36-40-1	200	336	29	854	830	2.38	2.88	0.40	4.8	3.07	1.015	21
S10-M-2.0-39-59-1	200	336	33	854	830	2.38	2.88	0.59	4.8	4.09	1.067	21
S10-M-2.0-36-89-1	200	336	29	854	830	2.38	2.88	0.89	4.8	4.00	1.111	21
210-0.19	200	336	23	1028	683	1.79	2.88	0.19	3.6	2.85	0.965	22
210-0.40	200	336	23	1028	683	1.79	2.88	0.40	3.6	4.28	1.027	22
210-0.59	200	336	23	1028	723	1.79	2.88	0.59	3.6	5.03	0.998	22
210-0.89	200	336	23	1028	723	1.79	2.88	0.89	3.6	5.69	1.008	22
210-1.15	200	336	23	1028	723	1.79	2.88	1.18	3.6	3.99	1.008	22
360-0.19	200	336	37	947	679	1.79	2.88	0.19	3.6	2.55	1.027	22
360-0.89	200	336	37	947	728	1.79	2.88	0.89	3.6	2.48	0.998	22
360-1.18	200	336	37	947	728	1.79	2.88	1.18	3.6	2.78	1.008	22
(2)-3	180	340	32	368	250	1.76	3.21	0.28	3.5	3.69	0.998	23
(2)-4	180	340	32	368	250	1.76	3.21	0.28	3.5	4.52	1.008	23
(2)-5	180	340	32	368	1324	1.76	3.21	0.28	3.5	4.89	1.027	23
(2)-7	180	340	32	368	250	1.76	3.21	0.56	3.5	6.29	1.008	23
(2)-8	180	340	32	368	250	1.76	3.21	0.56	3.5	4.68	0.965	23
(2)-11	180	340	32	368	255	1.76	3.21	0.75	3.5	2.64	1.027	23
(2)-13	180	340	32	368	255	1.76	3.21	1.13	3.5	5.28	0.998	23
(2)-15	180	340	32	368	674	1.76	3.21	0.29	3.5	2.72	1.008	23
(3)-2	180	340	28	343	329	2.35	3.21	0.19	4.7	3.22	1.042	23
(3)-4	180	340	28	343	329	2.35	3.21	0.26	4.7	3.99	1.015	23
(4)-3	180	340	20	795	1275	1.76	3.21	0.12	3.5	2.09	1.067	23
(4)-5	180	340	20	795	1238	1.76	3.21	0.19	3.5	4.14	0.965	23
(4)-7	180	340	20	795	1262	1.76	3.21	0.26	3.5	3.73	1.027	23
(4)-9	180	340	20	795	1353	1.76	3.21	0.37	3.5	2.17	0.998	23
(4)-10	180	340	20	795	285	1.76	3.21	0.26	3.5	5.66	1.008	23
(4)-12	180	340	20	795	274	1.76	3.21	0.59	3.5	2.70	1.071	23
(4)-14	180	340	20	795	258	1.76	3.21	0.83	3.5	2.39	0.959	23
(4)-16	180	360	20	795	1275	1.76	1.20	0.12	3.3	2.93	1.076	23
(4)-18	180	360	20	815	1275	1.76	0.61	0.12	3.3	5.58	1.088	23
E3H2(2-4)	152	326	25	395	314	1.99	2.60	0.89	7.9	2.90	1.055	24
C3H1(2-5)	152	316	20	412	316	2.05	2.68	1.11	8.2	2.96	1.024	24
C3H2(2-6)	152	315	20	410	316	2.06	2.69	0.89	8.2	4.63	1.064	24
E2A1(3-1)	152	318	25	313	345	2.23	2.67	0.37	8.2	5.41	1.009	24
E2A2(3-2)	152	318	19	305	345	2.23	2.67	0.37	8.2	3.11	1.010	24
E2A3(3-3)	152	316	20	325	349	2.24	2.68	0.37	8.2	4.70	1.035	24
C2A1(3-4)	152	318	23	304	353	2.23	2.67	0.37	8.2	2.52	1.045	24
C2A2(3-5)	152	311	21	309	347	2.27	2.72	0.37	8.3	2.06	1.021	24
E2H1(3-6)	152	324	21	400	347	2.18	2.61	0.82	8.0	3.30	0.921	24
E2H2(3-7)	152	309	20	412	361	2.29	2.74	0.52	8.4	3.31	0.983	24
C2H1(3-8)	152	311	22	404	352	2.27	2.72	0.82	8.3	3.86	0.974	24
C2H2(3-9)	152	325	25	399	356	2.17	2.60	0.52	8.0	6.37	1.011	24

References

[1] Russo G, Zingone G, Puleri G. Flexural–shear interaction model for longitudinally reinforced beams. ACI Structural Journal 1991;88(1):60–8.

[2] Fenwick RC, Paulay Sr T. Mechanisms of shear resistance of concrete beams. Journal of Structural Engineering, ASCE 1968;94(10):2325–50.

[3] Bazant ZP, Kim JK. Size effect in shear failure of longitudinally reinforced beams. ACI Structural Journal 1984;81(5):456–68.

[4] Russo G, Puleri G. Stirrup effectiveness in reinforced concrete beams under flexure and shear. ACI Structural Journal 1997;94(3):227–38.
[5] Placas A, Regan PE. Shear failure of reinforced concrete beams. ACI Journal, Proceedings 1971;68(10):763–73.
[6] Haddadin MJ, Hong S-T, Mattock AH. Stirrup effectiveness in reinforced concrete beams with axial force. Proceedings, ASCE 1971;97(ST9):2277–97.
[7] Elstner RC, Moody KG, Viest IM, Hognestad E. Shear strength of reinforced concrete beams. Part 3—tests of restrained beams with web reinforcement. ACI Journal, Proceedings 1955;51(6):525–39.
[8] ACI Committee 318, Building Code Requirements for Reinforced Concrete (ACI 318-02) and Commentary-ACI318RM-02, American Concrete Institute, Detroit, 2002.
[9] Canadian Standards Association, Design of Concrete Structures A23.3-94, Canadian Standards Association, Rexdale, Ontario, 1994.
[10] NZS 3101, The Design of Concrete Structures. Part 1, New Zealand Standards, Wellington, 1995.
[11] Vecchio FJ, Collins MP. The modified compression-field theory for reinforced concrete elements subjected to shear. ACI Structural Journal 1986;83(2):219–31.
[12] Hsu TTC. Softened truss model theory for shear and torsion. ACI Structural Journal 1988;85(6):624–35.
[13] Pang XB, Hsu TTC. Fixed angle softened truss model for reinforced concrete. ACI Structural Journal 1996;93(2):197–207.
[14] Lee JY, Kim SW, Mansour MY. Predicting the shear response of reinforced concrete beams using a new compatibility aided truss model. ACI Structural Journal, 2002, submitted for publication.
[15] Clark AP. Diagonal tension in reinforced concrete beams. ACI Journal, Proceedings 1951;48(2):145–56.
[16] Mattock AH, Wang Z. Shear strength of reinforced concrete members subject to high axial compressive stress. ACI Structural Journal 1984;81(3):287–98.
[17] Moretto O. An investigation of the strength of welded stirrups in reinforced concrete beams. ACI Journal, Proceedings 1945;42(2):141–62.
[18] Guralnick SA. High-strength deformed steel bars for concrete reinforcement. ACI Journal, Proceedings 1960;57(3):241–82.
[19] Kokusho S, Kobayashe K, Mitsugi S, Kumagai H. Ultimate shear strength of RC beams with high tension shear reinforcement and high strength concrete. Journal of the Structural Construction Engineering 1987;AIJ 373:83–91.
[20] Takagi H, Okude H, Nitta T. Shear strength of beam depending the strength of web reinforcements. Proceedings, JCI 1989;11(2):75–80.
[21] Nishiura N, Makitani E, Shindou K. Shear resistance of concrete beams with high strength web reinforcements. Proceedings, JCI 1993;15(2):461–6.
[22] Matsuzaki Y, Nakano K, Iso M, Watanabe H. Experimental study on the shear characteristic of RC beams with high tension shear reinforcement. Proceedings, JCI 1990;12(2):325–8.
[23] Fukuhara M, Kokusho S. Effectiveness of high tension shear reinforcement in reinforced concrete members. Journal of the Structural Construction Engineering 1982;AIJ 320:12–20.
[24] Rodriguez JJ, Bianchini AC, Viest IM, Kesler CE. Shear strength of two-span continuous reinforced concrete beams. ACI Journal, Proceedings 1959;55(10):1089–130.
[25] Bresler B, Scordelis AC. Shear strength of reinforced concrete beams, Series 100, Issue 13. Berkeley: Structures and Materials Research, Department of Civil Engineering, University of California; 1961.
[26] ACI-ASCE Committee 326. Shear and diagonal tension. ACI Journal, Proceedings 1962;59(1–3):1–30, 277–344, 352–96.
[27] Belarbi A, Hsu TTC. Constitutive laws of concrete in tension and reinforcing bars stiffened by concrete. ACI Structural Journal 1994;91(4):465–74.
[28] Belarbi A, Hsu TTC. Constitutive laws of softened concrete in biaxial tension–compression. ACI Structural Journal 1995;92(5):562–573.
[29] Zhu RH, Hsu TTC, Lee JY. Rational shear modulus for smeared crack analysis of reinforced concrete. ACI Structural Journal 2001;98(4):443–50.
[30] Rumelhart DE, McClelland JL, Parallel Distributed Processing Research Group. Parallel distributed processing explorations in the microstructure of cognition, vol. 1. 1st ed. Cambridge, MA: MIT Press, 1986.
[31] Hertz J, Krogh A, Palmer RG. Introduction to the theory of neural computing. Redwood City, CA: Addison-Wesley; 1991.
[32] Goh ATC. Prediction of ultimate shear strength of deep beams using neural networks. ACI Structural Journal 1995;92(1):28–32.
[33] Teh CI, Wong KS, Goh ATC, Jaritngam S. Prediction of pile capacity using neural networks. Journal of Computing in Civil Engineering, ASCE, 1997;11(2):129–138.
[34] Sanad A, Saka MP. Prediction of ultimate shear strength of reinforced concrete deep beams using neural networks. Journal of Structural Engineering, ASCE 2001;127(7):818–28.
[35] Oreta AWC, Kawashima K. Neural network modeling of confined compressive strength and strain of circular concrete columns. Journal of Structural Engineering, ASCE 2003;129(4):554–61.
[36] Hammerstorm D. Working with neural networks. IEEE Spectrum 1993;46–53.
[37] Zhang J. Performance-based seismic design using designed experiments and neural networks. PhD dissertation, Department of Civil Engineering, University of British Columbia, B.C. Canada, April 2003.
[38] Patterson DW. Artificial neural networks, theory and applications. Prentice Hall, 1995. 477 pp.
[39] Hornik K, Stinchcomebe M, White H. Multilayer feedforward networks are universal approximators. Neural Networks 1989;2(3):356–66.
[40] Swingler K. Applying neural networks a practical guide. New York: Academic Press; 1996.
[41] Rafiq MY, Bugmann G, Easterbrook DJ. Neural network design for engineering applications. Computers and Structures 2001;79:1541–52.
[42] Stein R. Selecting data for neural networks. AI Expert 1994;2:42–7.
[43] Zsutty TC. Shear strength prediction for separate categories of simple beam test. ACI Journal 1971;68(2):138–43.
[44] Propagator: version 1.0, A. R. D. Environmental Inc., Md., 1996.
[45] Predict Professional, Neural Ware Inc., Pittsburgh, PA, 1997.